Pseudo-stochastic simulation of turbulent channel flows with near-wall modelling

Carlo Cintolesi, Etienne Mémin

Pseudo-stochastic simulation of turbulent channel flows with near-wall modelling

Carlo Cintolesi[a,*], Etienne Mémin[a]

[a] *INRIA Rennes - Bretagne Atlantique, Fluminance group, Campus de Beaulieu, F-35042 Rennes, France*

Abstract

The pseudo-stochastic model recently proposed by Mémin (2014) is investigated and compared with the large-eddy simulation methodology. The theoretical analysis shows that this model is a generalisation of the eddy-viscosity model, which does not undergo the same restrictive physical assumptions and describes physical phenomena usually not considered (turbophoresis and turbulent compressibility). Numerical simulations of turbulent channel flows are performed. In order to better reproduce the turbulence anisotropy, a near-wall damping function is derived and successfully validated: the damping is imposed only on wall-normal direction (minimal constraint) and it requires to set a single parameter (reduced empirical content). Simulations show the accuracy of the new model, especially when the computational grid becomes coarse. A weak turbophoresis phenomenon is detected near the wall, while turbulent compressibility effects appear to be possibly related to the streaks structures.

Keywords: Stochastic model, Turbulence, Near-wall models, Numerical simulations, OpenFOAM.

1. Introduction

The use of stochastic calculus to describe fluid flows appears to be a suitable strategy for turbulence modelling in computational fluid dynamics. The random nature of turbulence cannot be completely represented by means of deterministic variables, while it is the specific purpose of stochastic processes. Nevertheless, the numerical solution of stochastic equations and the mathematical complexity inherent to the use of stochastic calculus poses challenging issues. Turbulence modelling with stochastic variables is of great interest in geophysical flow analysis, where the unresolved processes related to coarse spatial discretisation are handled with probabilistic models. In the same spirit, stochastic models can be applied to numerical simulations of environmental and engineering flows.

*Corresponding author

Email addresses: carlo.cintolesi@gmail.com (Carlo Cintolesi), etienne.memin@inria.fr (Etienne Mémin)

In the last decades, several efforts have been made in this concern. In the context of the Probability Density Function (PDF), the Langevin equation was used to describe the velocity of a fluid particle subject to a turbulent flow, modelled as a Brownian motion (see Pope (2000)). First applications focused on homogeneous isotropic turbulence; later extended by Pope (1983) to inhomogeneous case and by Durbin and Speziale (1994) to anisotropic diffusion case. In the Eddy-Damped Quasi-Normal Markovian (EDQNM) models, introduced by Orszag (1970) and Leslie (1973), the large-scale governing equations were closed in the spectral space by modelling the third/fourth-order moments through a Gaussian closure. This strategy was found to be suitable in case of strong non-linearity in the small-scale turbulence. Chasnov (1991) developed a forced-dissipative model, where the large-eddy Navier-Stokes equations were corrected by an eddy-viscosity and a stochastic force terms. Similarly, Leith (1990) studied the case of plane shear mixing layer and improved the accuracy of LES with the Smagorinsky model by adding an empirical stochastic backscatter. The work of Kraichnan (1961) exploited a different approach: the Navier-Stokes equations were replaced by a set of equations having the same mathematical properties, closed by a Gaussian stochastic model. This model led to valuable results when applied to the study of mathematical properties and physical effects, like turbulent diffusion and backscatter. Frederiksen et al. (2013) showed that the same methodology can be used in the stochastic modelling of barotropic flows or in quasi-geostrophic approximation, as well as for the description of the interactions between topography and small-scale eddies.

Such attempts to include random functions in fluid dynamics modelling exhibit some limitations: in POF and EDQNM models the solution is found in the spectral space instead of the physical one; the explicit introduction of random term relies mostly on empirical considerations and leads to a certain degree of arbitrariness. For example, a question arises whether the random forcing term should be multiplicative or additive.

An alternative approach was developed. It is based on the idea that the velocity field itself is a random process, composed of a differentiable component and a fast oscillating random term. Physically, the former describes the smooth macroscopic velocity while the latter accounts for the stochastic turbulent motion. Under this assumption, the fluid dynamics equations are re-derived using stochastic calculus, leading to a complete set of stochastic partial differential equations. Pioneering work in this sense was made by Brzeźniak et al. (1991). Subsequently, Mikulevicius and Rozovskii (2004) and Flandoli (2011) expanded his formulation and studied the mathematical properties of the resulting stochastic system. Such a model has been further developed by Mémin (2014) in view of practical applications and takes the name of model under Location Uncertainty (LU). Later, Neves and Olivera (2015) theoretically investigate a similar system, while Holm (2015) derives an equivalent model using Lagrangian mechanics. This last model differs from LU because an extra term appears in the momentum equation, which ensures helicity and circulation conservation but may alter the kinetic energy budget.

The LU model was tested in several cases: Resseguier et al. (2017a,b,c) successfully used such type of model to study geophysical flows, which was found to be more accurate in the reproduction of extreme events and provided new analysis tools. Chapron et al. (2017) investigated the Lorentz-63 case and state that LU is more effective in exploring the regions of the deterministic attractor than the classical models. Furthermore, it was used in conjunction with the proper orthogonal decomposition technique by Resseguier et al. (2017d) for studying a wake flow past a circular cylinder at $Re = 3900$. Recently, Pinier et al. (2019) perform mathematical analysis of the turbulent boundary layer through the LU equations. They propose a complete explicit profile for the mean vertical velocity, that includes an expression for the velocity in the buffer layer, for which a rigorous theoretical model is missing so far.

Despite these encouraging results, to perform stochastic numerical simulations for practical applications poses some difficulties; e.g. the numerical resolution techniques are not straightforward and they can possibly require a large computational effort. In order to circumvent such difficulties, Mémin (2014) introduced a hybrid model hereafter named *pseudo-stochastic model*: first, the governing equations are decomposed into two coupled system of partial and stochastic differential equations; second, the resolution of the latter is avoided and the system is closed by modelling the effects of the random velocity term through physical assumptions. Hence, the flow dynamics is described by a set of classical partial differential equations, which includes terms that derive from the stochastic representation of turbulence. Harouna and Mémin (2017) used the pseudo-stochastic model to investigate the Green-Taylor vortex flow, testing several closure models. Chandramouli et al. (2018) successfully employed the model to simulate the transitional wake flow with coarse mesh resolution.

The present contribution aims to explore the potentiality of the pseudo-stochastic model, making a direct comparison with the Large-Eddy Simulation (LES) methodology. First, the model is described and discussed in details; then numerical simulations on the turbulent channel flows are performed and analysed. The main novelties here reported are: a detailed study of the pseudo-stochastic equations with respect to the classical ones; the derivation of a (resolved) turbulent kinetic energy budget for LU; the development of a near-wall model for pseudo-stochastic simulations from the study carried out by Pinier et al. (2019).

The paper is organized as follows: section 2 describes the pseudo-stochastic equations, along with the kinetic energy budget and the near-wall model; section 3 reports a physical interpretation of the equation terms, as well as a comparison with the LES methodology; section 4 presents the simulation methodologies and settings; section 5 discusses the validation of the near-wall model and the simulation results; section 6 reports some final remarks.

2. Pseudo-stochastic model

The pseudo-stochastic equations are described, together with the kinetic energy budgets. We refer to Mémin (2014) and Resseguier (2017) for the formal derivation.

2.1. Stochastic formalism

The pathlines in a turbulent flow are modelled as a stochastic process, where a regular function is perturbed by a random (turbulent) process. Consequently, a Lagrangian fluid-particle displacement is described by a stochastic differential equation of the type:

$$dX_t^i(x_0) = w_i(X_t, t)dt + \int_\Omega \sigma_{ik}(X_t, y, t)dB_t^k(y)\, dy, \tag{1}$$

where the index $i = 1, 2, 3$ indicates respectively the x,y,z-component in the space domain Ω (they are placed at top or bottom indifferently) and the Einstein summation convention is adopted; X_t^i is the trajectory followed by a fluid-particle initially located in x_0; w_i is a differentiable function that corresponds to the drift velocity; $d\eta_t^i = \int_\Omega \sigma_{ik} dB_t^k dy$ is a stochastic process (accounting for turbulent effects) uncorrelated in time but correlated in space. This last is constructed as a combination of a cylindrical Wiener processes $B_t^k(x)$ not differentiable in time, and a time-differentiable symmetric *diffusion tensor* $\sigma_{ik}(x, y, t)$ which acts as an integral kernel. Hence, they are fast oscillating stochastic components, possibly anisotropic and inhomogeneous in space.

The velocity field U_i in Eulerian coordinate x is derived from equation (1):

$$U_i(x, t) = w_i(x, t) + \dot{\eta}_t^i(x), \tag{2}$$

where the second term on the right-hand side expresses the stochastic velocity defined as the weak derivative of $\eta_t^i(x)$ in time. From a physical point of view, w_i is the velocity expected value and $\dot{\eta}_t^i(x)$ represents a noise: a generalised stochastic process that has to be defined in the space of temperate distribution, see Øksendal (2003).

In the derivation of the stochastic model, the quadratic variation of the diffusion tensor is of particular interest since it represents the time-variation of spatial variance of the stochastic increments along time. It is named as the *variance tensor* and it is defined as:

$$a_{ij}(x, t) = \int_\Omega \sigma_{ik}(x, y, t)\sigma_{kj}(x, y, t)\, dy, \tag{3}$$

it can be shown to be a symmetric and semi-positive definite matrix with dimension $[m^2/s]$.

2.2. Pseudo-stochastic equations of motion

The stochastic process (1) that described the flow is not time-differentiable in the framework of classical analysis. Thus, the Navier-Stokes equations need to be re-derived using the stochastic calculus, where the use of the Itō-Wentzell formula is crucial for computing the derivative in time, see Kunita (1997). The result is a complete system of stochastic partial differential equations that describes the fluid flow. Assuming the drift velocity is of bounded variation (deterministic) and using the unique decomposition of semi-martingale, the system can be divided into a set of stochastic equations and a set of pure deterministic ones. The former allows finding an expression for the variance tensor a_{ij}, required for the resolution of the latter. The pseudo-stochastic model is derived by neglecting the resolution of the stochastic equations and closing the system by giving an expression of the variance tensor, which is modelled through physical hypothesis. This choice gives rise to a hybrid model where the terms that depend on a_{ij} accounts for the *Stochastic Unresolved Scales* (SUS) of motion.

The pseudo-stochastic equations for incompressible flows read:

$$\begin{cases} \dfrac{\partial w_i}{\partial t} + w_j^* \dfrac{\partial w_i}{\partial x_j} = -\dfrac{\partial p}{\partial x_i} + \nu \dfrac{\partial^2 w_i}{\partial x_j \partial x_j} + \dfrac{1}{2} \dfrac{\partial}{\partial x_j} \left(a_{jk} \dfrac{\partial w_i}{\partial x_k} \right) \\ \dfrac{\partial w_i^*}{\partial x_i} = 0. \end{cases} \tag{4}$$

they represent the momentum and mass conservation, respectively, written in the non-conservative form proposed by Resseguier et al. (2017a). The *effective advection* velocity w^* is defined as:

$$w_i^* = w_i - \frac{1}{2} \frac{\partial a_{ik}}{\partial x_k}, \tag{5}$$

and the pressure is the sum of an hydrostatic pressure and an isotropic turbulent term:

$$p = p_h + \frac{\nu}{3} \frac{\partial w_\ell}{\partial x_\ell} = p_h + \frac{\nu}{6} \frac{\partial^2 a_{sk}}{\partial x_k \partial x_s}. \tag{6}$$

This last term does not contribute to the flow and it is included in the pressure gradient in the same manner as the isotropic residual stress in the Smagorinsky model, see Pope (2000).

It is worthwhile to notice that system (4) reduces to the classical Navier-Stokes equations when the variance tensor tends to the zero matrix, i.e. when the stochastic contributions disappear.

In the framework of computational fluid dynamics, the drift velocity w_i can be interpreted as the (numerically) resolved velocity field, while the random field η_t^i assembles the (turbulent) unresolved motions. Therefore, giving an expression on variance tensor is equivalent to specifying a turbulence model.

2.3. Resolved kinetic energy budget

Equations for mean and turbulent kinetic energy budget of the resolved scales of motion are here derived. The resolved velocity is decomposed in a mean and a fluctuating part, respectively:

$$w_i = W_i + w_i', \tag{7}$$

where the capital letter indicates the averaged field, $W_i = \langle w_i \rangle$. Variance tensor and pressure are decomposed in a similar way: $a_{ij} = A_{ij} + a_{ij}'$ and $p = P + p'$. The variance tensor accounts for the SUS effects on the mean flow.

The budget of resolved kinetic energy $K = (W_i W_i)/2$ is obtained multiplying momentum equation (4-first) by W_i and averaging. Applying the conservation of mass (4-second) and rearranging the terms, one gets:

$$\frac{\partial K}{\partial t} + \left(W_j - \frac{\partial}{\partial x_k}\frac{A_{jk}}{2}\right)\frac{\partial K}{\partial x_j} = \frac{\partial}{\partial x_j}\Big[- PW_j + (\nu\delta_{jk} + \frac{A_{jk}}{2})\frac{\partial K}{\partial x_k} \tag{8}$$

$$- \langle\left(w'_j - \frac{\partial}{\partial x_k}\frac{a'_{jk}}{2}\right) w'_i\rangle W_i + \langle a'_{jk}\frac{\partial w'_i}{\partial x_k}\rangle W_i\Big] \tag{9}$$

$$+ \frac{p'}{2}\frac{\partial^2 A_{jk}}{\partial x_j \partial x_k} - \left(\nu\delta_{jk} + \frac{A_{jk}}{2}\right)\frac{\partial W_i}{\partial x_j}\frac{\partial W_i}{\partial x_k} \tag{10}$$

$$+ \langle\left(w'_j - \frac{\partial}{\partial x_k}\frac{a'_{jk}}{2}\right) w'_i\rangle\frac{\partial W_i}{\partial x_j} - \langle\frac{a'_{jk}}{2}\frac{\partial w'_i}{\partial x_j}\rangle\frac{\partial W_i}{\partial x_k} \tag{11}$$

The second term on the left-hand side represents the rate of change by means of the effective (mean) advection. The first four terms on the right-hand side express the energy transport by pressure, molecular and turbulent viscous stresses, resolved turbulence, turbulent SUS motion (respectively). The fifth term is due to the non-solenoidal velocity field and is related to the compression-expansion work made by the SUS; it can be a production or dissipation term. The sixth term is a viscous and turbulent dissipation (it can be proven that A_{ij} is positive defined), while the seventh term is a loss due to resolved turbulence; the same term but with opposite sign is present in the turbulent kinetic energy budget presented later in this section. The last term indicates dissipation/production due to SUS.

The (resolved) turbulent kinetic energy $\kappa = w'_i w'_i/2$ budget is obtained following the procedure described in Kundu and Cohen (2004): the equation for resolved fluctuations is obtained subtracting expression (8) from (4-first), then multiplying by w_i and averaging. Using the continuity equation (4-second) to simplify the terms and rearranging them, one obtains the following expression for stochastic Turbulent Kinetic Energy (TKE):

$$\frac{\partial\langle\kappa\rangle}{\partial t} + \underbrace{\left(W_j - \frac{\partial}{\partial x_k}\frac{A_{jk}}{2}\right)\frac{\partial\langle\kappa\rangle}{\partial x_j} + \langle\left(w'_j - \frac{\partial}{\partial x_k}\frac{a'_{jk}}{2}\right)\frac{\partial\kappa}{\partial x_j}\rangle}_{advection} =$$

$$= \underbrace{\frac{\partial}{\partial x_j}\left[-\langle p' w'_j\rangle + \left(\nu\delta_{jk} + \frac{A_{jk}}{2}\right)\frac{\partial\langle\kappa\rangle}{\partial x_j} + \langle\frac{a'_{jk}}{2}\frac{\partial\kappa}{\partial x_j}\rangle + \langle\frac{a'_{jk}w'_i}{2}\rangle\frac{\partial W_i}{\partial x_k}\right]}_{transport}$$

$$+ \underbrace{\langle\frac{p'}{2}\frac{\partial^2 a'_{jk}}{\partial x_j \partial x_k}\rangle}_{turb.\ compress.} - \underbrace{\left(\nu\delta_{jk} + \frac{A_{jk}}{2}\right)\langle\frac{\partial w'_i}{\partial x_j}\frac{\partial w'_i}{\partial x_k}\rangle - \langle\frac{a'_{jk}}{2}\frac{\partial w'_i}{\partial x_j}\frac{\partial w'_i}{\partial x_k}\rangle}_{dissipation}$$

$$- \underbrace{\langle\left(w'_j - \frac{\partial}{\partial x_k}\frac{a'_{jk}}{2}\right) w'_i\rangle\frac{\partial W_i}{\partial x_j}}_{production} - \underbrace{\langle\frac{a'_{jk}}{2}\frac{\partial w'_i}{\partial x_j}\rangle\frac{\partial W_i}{\partial x_k}}_{loss\ to\ SUS} \tag{12}$$

On the left-hand side, the second and third terms represent the TKE advection by mean and SUS effective advection velocity, respectively. On the right-hand side:

- the first four terms express spatial transport;
- the fifth term is a turbulent compression/expansion term due to SUS;
- the sixth and seventh terms account for dissipation by molecular viscosity, resolved turbulence and SUS motions;
- the eight term represents the shear production, including the contribution by the fluctuations of turbulent advection velocity;
- the last term indicates a loss due to SUS; this term is also present in the resolved kinetic energy budget.

Both the kinetic energy and TKE expressions reduce to the classical ones if the stochastic contribution is negligible $a_{ij} \simeq 0$.

2.4. Isotropic constant model for variance tensor

Several strategies can be adopted to model the variance tensor. The isotropic model is developed by analogy with the Smagorinsky model, e.g. see Deardorff (1970), and was first proposed by Mémin (2014). The variance tensor is given by:

$$a_{ij} = c_m \Delta^2 \left| S \right| \delta_{ij}, \tag{13}$$

where c_m is a model parameter, $|S|$ is the strain-rate tensor norm, and Δ is the computational cell width. The variance tensor reduces to a diagonal matrix with equal elements because turbulence is assumed isotropic and homogeneous in all directions.

2.5. Near-wall modelling of variance tensor

In a very recent work, Pinier et al. (2019) studied the mean velocity profile of the turbulent boundary layer through the LU equations. They proposed a modification of the classical velocity expression for wall-bounded flow and provided an analytical formula for the buffer layer, not available till now. Notice that the modified advection velocity plays a crucial role in the mathematical derivation of this formula; therefore, such a profile cannot be deduced using the classical formulation of the Navier-Stokes equations, where the modified advection is not explicitly taken into account. In the viscous sublayer ($y^+ < y_0^+$) and in the logarithm region ($y_L^+ < y^+ < y_1^+$) the linear and log-law velocity profiles (respectively) are retrieved, while in the buffer layer ($y_0^+ < y^+ < y_L^+$) a hyperbolic profile is specified:

$$u^+(y^+) = \begin{cases} y^+ & y^+ \in [0, y_0^+] \\ u^+(y_0^+) + \dfrac{2}{\widetilde{\kappa}} - \dfrac{4}{\widetilde{\kappa}\left[(\widetilde{\kappa} y^+ - y_0^+) + 2\right]} & y^+ \in [y_0^+, y_L^+] \\ u^+(y_L^+) + \dfrac{4 y_L^+}{\left[\widetilde{\kappa}(y_L^+ - y_0^+) + 2\right]^2} \ln\left(\dfrac{y^+}{y_L^+}\right) & y^+ \in [y_L^+, y_1^+] \end{cases} \tag{14}$$

where $u(y)$ is the streamwise velocity as a function of the wall-normal coordinate. Quantities are made non-dimensional by means of the friction velocity u_τ and molecular viscosity ν, as usual: $y^+ = yu_\tau/\nu$ and $u^+ = u/u_\tau$. The $\widetilde{\kappa}$ is a model constant (to not be confused with the von Kármán constant); for a plain channel flow it has been estimated to be $\widetilde{\kappa} = 0.158$ from direct numerical simulations. The boundaries of the three regions are: $y_0^+ \simeq 5$, $y_L^+ \simeq 50$, and $y_1^+ \simeq 150$ even if the profile is often extended till the half of the channel. Let us stress that these profiles are rigorously derived from the LU models. See Pinier et al. (2019) for an extensive validation on the pipe flow, turbulent boundary layer, and channel flows.

An additional result concerns the expression of the variance tensor. In the viscous sublayer, a_{ij} is almost zero, while in the buffer layer the wall-normal component depends only from the distance from the wall and exhibits a linear profile:

$$a^+_{yy}(y^+) = \widetilde{\kappa}\left(y^+ - y_0^+\right), \tag{15}$$

where $a^+_{ij} = a_{ij}/\nu$. In the log-law region, it scales as the square-root of the wall distance:

$$a^+_{yy}(y^+) = \widetilde{\kappa}\left(y_L^+ - y_0^+\right)\sqrt{y^+/y_L^+}. \tag{16}$$

No estimations are provided for the other components.

Preliminary pseudo-stochastic simulations with the isotropic constant model (13) have shown an excessive energy dissipation near the solid boundaries, given by high values of a_{ij} in the buffer and viscous layer. This is not unexpected since the LES Smagorinsky model (that is the classical counterpart of the isotropic model) exhibit the same behaviour (see discussion in following section 3.2).

To correct this behaviour, a damping function for variance tensor is here formulated, exploiting the above-described characterisation of wall-normal component. Away from the wall, a_{yy} is given by the isotropic model; at a point y_B^+ placed in the buffer layer, a linear decrease is imposed in such a way to reach the zero value at y_0^+; in the viscous sublayer, it is set to be zero. Hence, the LU near-wall model reads:

$$a^+_{yy}(y^+) = \begin{cases} 0 & y^+ \in [0, y_0^+] \\ a^+_{yy}(y_B)\dfrac{y^+ - y_0^+}{y_B^+ - y_0^+} & y^+ \in [y_0^+, y_B^+] \\ \dfrac{c_m \Delta^2}{\nu}\,|S|\,\delta_{ij} & y^+ \in [y_B^+, y_1^+] \end{cases} \tag{17}$$

The coordinate y_B^+ is a model parameter that have to be set after theoretical or numerical estimation. No constraints are imposed on the other components; they are computed according to the isotropic model (13).

3. Physical interpretation and comparison with LES models

The pseudo-stochastic equations (4) are analysed from a physical point of view, and a comparison with the eddy-viscosity model used in LES is reported.

3.1. Physical interpretation

Recalling the decomposition of the velocity gradient as the sum of the symmetric and the antisymmetric part, respectively the strain-rate tensor $S_{ij} = \frac{1}{2}\left(\partial w_i/\partial x_j + \partial w_j/\partial x_i\right)$ and the rotation-rate tensor $\Omega_{ij} = \frac{1}{2}\left(\partial w_i/\partial x_j - \partial w_j/\partial x_i\right)$, the pseudo-stochastic equations (4) are rearranged as:

$$\frac{\partial w_i}{\partial t} + \left(w_j - \frac{1}{2}\frac{\partial a_{jk}}{\partial x_k}\right)\frac{\partial w_i}{\partial x_j} = -\frac{\partial p}{\partial x_i} + \frac{\partial}{\partial x_j}\left[\left(2\nu\delta_{jk} + \frac{a_{jk}}{2}\right)S_{ki}\right] - \frac{\partial}{\partial x_j}\left(\frac{a_{jk}}{2}\Omega_{ki}\right), \tag{18}$$

and

$$\frac{\partial w_i}{\partial x_i} = \frac{1}{2}\frac{\partial^2 a_{jk}}{\partial x_j \partial x_k}. \tag{19}$$

The terms that depend on variance tensor account for the influence of the SUS on the resolved scales. A physical interpretation of such terms is proposed:

Effective advection: the advection velocity is corrected by an inhomogeneous turbulence contribution. As pointed out by Resseguier et al. (2017a), it corresponds to a velocity induced by the unresolved eddies, that is linked to the *turbophoresis* phenomenon detectable in geophysical flows; i.e. the tendency of fluid-particle to migrate in the direction of less energetic turbulence.

Diffusion due to SUS: the last two terms on the right-hand side of equation (18) account for the turbulent diffusion; the variance tensor plays the role of a diffusion tensor similar to a generalised eddy-viscosity coefficient. Both the deformation rate and rotation-rate contribute to diffusion, unlike in the classical eddy-viscosity model in which fluid rotation-rate is assumed to be irrelevant in turbulent modelling.

Turbulent compressibility: the continuity equation (19) suggests that the flow is turbulent-compressible; i.e. the unresolved turbulence induces a local fluid compression or expansion.

The variance tensor (3) is the key parameter of the pseudo-stochastic model. It has the physical dimension of a dynamic viscosity $[m^2/s]$, and carries information on the intensity of the SUS. The role played in governing equations (4) and in kinetic energy budgets (8)-(12), suggests that a_{ij} can be interpreted as a generalised eddy-viscosity parameter. Implicitly, this leads to the hypothesis that the SUS influences the resolved flow as an alteration (increasing or possibly decreasing) of fluid viscosity, which is an empirical consideration largely accepted.

The divergence of the variance tensor is hereafter named turbulent advection velocity:

$$u_{\mathrm{TA},i} = -\frac{1}{2}\frac{\partial a_{ij}}{\partial x_j}; \tag{20}$$

the divergence of the turbulent advection velocity measures the turbulent compressibility:

$$\Phi_{\text{TC}} = \frac{1}{2}\frac{\partial^2 a_{ij}}{\partial x_i \partial x_j}, \tag{21}$$

and it is directly proportional to the isotropic turbulent term appearing in equation (6).

3.2. Comparison with LES eddy-viscosity models

In the classical framework, the fluid velocity $u(x,t)$ is a deterministic function of time and space. Adopting the LES approach, the computational grid act on the governing equations as an implicit spatial filter (denoted by an over-bar) depending on the local cell width $\Delta = (\Delta x \Delta y \Delta z)^{1/3}$, see Sagaut (2000) and Piomelli (2001) for extended reviews. Filtering the Navier-Stokes equations, the sub-grid scale (SGS) stress tensor $\tau_{ij} = (\overline{u}_i \overline{u}_j - \overline{u_i u_j})$ appears:

$$\begin{cases} \dfrac{\partial \overline{u}_i}{\partial t} + \overline{u}_j \dfrac{\partial \overline{u}_i}{\partial x_j} = -\dfrac{\partial \overline{p}}{\partial x_i} + \nu \dfrac{\partial^2 \overline{u}_i}{\partial x_j \partial x_j} - \dfrac{\partial \tau_{ij}}{\partial x_j} \\ \dfrac{\partial \overline{u}_i}{\partial x_i} = 0 \end{cases} \tag{22}$$

and it has to be modelled to close the system: a popular choice is to use the eddy-viscosity models. They are a class of turbulent models relying on the Boussinesq assumption, where the anisotropic part of τ_{ij} is proportional to the resolved strain-rate tensor through ν_{SGS} the SGS viscosity parameter:

$$\tau_{ij}^R = \tau_{ij} - \frac{\tau_{kk}}{3}\delta_{ij} = -2\nu_{\text{SGS}}\overline{S}_{ij}, \tag{23}$$

while the isotropic part is included in the pressure term and does not contribute to the motion. This parameter has to be specified by additional models; the classical constant Smagorisky model is here analysed:

$$\nu_{\text{SGS}} = c_s^2 \Delta^2 \left|\overline{S}\right|, \tag{24}$$

where $\left|\overline{S}\right|$ is the norm of the filtered strain-rate tensor, and the parameter c_s^2 is set constant and can be evaluated from experiments, direct numerical simulations or analytical considerations, e.g. see Lilly (1967). The main drawback of this approach is to rely on the homogeneous turbulence assumption. This hypothesis is violated in many, even simple, cases. For example, close to solid surfaces where the turbulent length-scales decrease. To cope with this shortcoming, a damping function is usually introduced in order to account for the reduction of turbulence intensity. After the first work of van Driest (1956) several modifications of the original damping function have been proposed, e.g. see Piomelli et al. (1989) Cabot and Moin (2000). They can be summarised in the following expression:

$$\widetilde{\Delta} = \min\left\{\frac{\kappa y}{C_\delta}\left[1 - e^{\left(-\frac{y^+}{A^+}\right)^n}\right]^m, \Delta\right\}, \tag{25}$$

where $\kappa = 0.41$ is the von Kármán constant. The original formulation by van Driest (1956) prescribe $n = m = 1$, $A^{+} = 0.26$ and $C_{\delta} = 1.00$.

Remarks on eddy-viscosity model

Notice that the eddy-viscosity equation (23) implies that the Boussinesq's hypotheses are satisfied: (a) the anisotropic Reynolds stress tensor is aligned with the mean strain-rate tensor; (b) the two are directly proportional through a single parameter, equal for all the six independent components of τ_{ij}^{R}.

The pseudo-stochastic model is equivalent to an eddy-viscosity model if the variance tensor is expressed by $a_{ij} = 2\nu_{\text{SUS}}\delta_{ij}$, i.e. assuming that the SUS induce an (isotropic) increasing of fluid viscosity. In this sense, the pseudo-stochastic model can be considered as a generalisation of the eddy-viscosity model. The comparison between the two models points out some theoretical advantages of the former:

(i) The effects of unresolved scales of motion are given by a_{ij}, without imposing any constraints on the directions along with the SUS acts on the resolved flow. Hence, hypothesis (a) is not required.

(ii) The tensor form of a_{ij} allows reproducing the anisotropy of unresolved turbulence, i.e. different turbulent contributions along different directions. Thus, hypothesis (b) is not required.

(iii) The extra terms in the governing equations account for turbulent effects usually not considered in the classical models, namely turbulent advection and turbulent compressibility.

The eddy-viscosity models are reasonable for simple shear flows and it is largely applied in computational fluid dynamics. However, most of their shortcomings derive from the fact that hypotheses (a) and (b) are not generally satisfied; see Pope (2000) for an overview on this issue.

It is worth mentioning that the eddy-viscosity parameter a_{ij} comes directly from the basic assumption of the velocity decomposition (2); whereas it is introduced in LES equations through an *ad hoc* physical assumption. Overall, the pseudo-stochastic model represents a general approach that overcomes the limitations of the Boussinesq assumption and includes turbulent effects not considered in the classical LES sub-grid scales models.

Remarks on Smagorinsky model

Expanding the pseudo-stochastic isotropic model (13), it can be shown that it reduces to the LES Smagorinsky model under two approximations:

(i) the rotation-rate does not contribute to turbulence effects on the mean flow;

(ii) the norm of the strain-rate tensor is almost harmonic (Laplacian is close to zero).

Notice that with the latter hypothesis the continuity equation (4-second) boils down to the classical solenoidal constraint. Therefore, the LES Smagorinsky model can be interpreted as a particular case of the pseudo-stochastic isotropic model.

Approximation (i) is valid if the turbulent energy is mainly concentrated in the region where the irrotational strain dominates vorticity. Exceptions on this behaviour have been found and have motivated the development of alternative models, like the *wall adaptive local-eddy viscosity* (WALE) model of Nicoud and Ducros (1999) or the structure function model of Métais and Lesieur (1992). Approximation (ii) implies that the flow deformation rate can be represented by a linear function in each spatial point; thus it is a particularly regular function. This is equivalent to neglect the turbulent correction on advective velocity and continuity equation, hence the associated physical phenomena of turbophoresis and turbulent compressibility are not reproduced.

4. Simulation methodologies

The LU near-wall model (17) is validated on turbulent plain channel flow at $Re_\tau = 395$. Subsequently, the pseudo-stochastic model is studied in detail on channel flow at $Re_\tau = 590$. Several simulations are performed changing the computational grid resolution, and the results of *pseudo-stochastic simulation* (PSS) are compared with a LES and the *direct numerical simulation* (DNS) of Moser et al. (1999).

4.1. Methodology and implementation

Simulations are performed taking advantage of the open-source software OpenFOAM v6. This is a C++ library for computational fluid dynamics and uses the finite volume method.

The LESs are carried out using the solver `pisoFoam` included in the standard software distribution. The implementation details can be found in the OpenFOAM documentation and in Jasak et al. (1999). The filtered classical Navier-Stokes equations are closed by the Smagorinsky model (24), with $c_s = 0.65$. The van Driest function (25) for near-wall damping is used unless otherwise specified. The optimal parameters are set as $n = m = 1$, $A^+ = 0.26$, $C_\delta = 0.158$, which lead to a formulations similar to the original one by van Driest (1956).

The PSSs are carried out using the home-made solver `pseudoStochasticPisoFoam`, developed by the authors at the Fluminance research group at INRIA Rennes (France). The pseudo-stochastic equations (4) are solved employing the Pressure-Implicit with Splitting of Operators (PISO) algorithm proposed by Issa et al. (1986) and Oliveira and Issa (2001). The variance tensor is expressed by the isotropic constant model (13), corrected by the near-wall damping function (17) unless otherwise specified. The model constant is set to be $c_m = 2c_s^2$ in analogy with the Smagorinsky model. The damping parameter is set to be $y_B^+ = 2/\tilde{\kappa} = 12.7$ after a theoretical estimation, confirmed by several test simulations. In order to regularise the damped profile of a_{yy}, a smoothing filter is applied to the variance tensor.

Re_τ	Mesh	grid points	$y^+_{wall} \div \Delta y^+_{max}$	Δx^+	Δz^+	λ
395	FINE	$50 \times 80 \times 80$	$0.71 \div 25$	50	23	5.00
590	FINE	$96 \times 96 \times 96$	$0.71 \div 36$	40	20	5.25
	COARSE	$64 \times 64 \times 64$	$1.14 \div 48$	58	29	5.20
	VERY COARSE	$32 \times 64 \times 32$	$1.14 \div 48$	116	58	5.20

Table 1: Computational grid settings for numerical simulations of turbulent channel flow. The y^+_{wall} is the coordinate of the first point near the wall.

Variables are discretised in space with a second-order central difference scheme, while time integration is performed using an implicit Euler backward scheme. Such a scheme employs the variables at the previous two time steps, leading to a second order accuracy. Globally, numerical solvers are second-order accurate in time and space. The time advancement fulfils the Courant-Friedrichs-Lewy condition $Co < 0.5$. For LES, the Courant number is computed as $Co = \Delta t|u|/\delta x$, where Δt is the time step, $|u|$ is the velocity magnitude through the cell, δx is the cell length. For PSS, the definition is modified in order to account for the effective advection velocity: $Co = \Delta t|w^*|/\delta x$.

4.2. Case geometry and settings

The channel is composed of two horizontal and parallel walls between which a shear flow develops. The dimensions in stream-wise (x), vertical (y) and span-wise (z) directions are $2\pi\delta \times \delta \times \pi\delta$, respectively. Several discretisation meshes are employed, whose parameters are summarised in Table 1. The computational points are uniformly distributed in streamwise and spanwise directions, while the grid is stretched along the vertical direction. The stretching is symmetric with respect to the channel center plane $y = \delta$, and it is obtained with a double-side stretching function based on hyperbolic tangent:

$$y(\xi) = \frac{1}{2}\left(1 + \frac{\tanh(\lambda(\xi - 1/2))}{\tanh(\lambda/2)}\right), \tag{26}$$

where ξ is the vertical coordinate of uniform point distribution. The fine meshes are such that the first cell is within $y^+ = 1$ and with 9 cells in $y^+ \leq 11$, and the cell width in the wall-parallel plane are sufficient to ensure an accurate resolution of the boundary layer. The coarse and very coarse meshes still have a good vertical resolution but the streamwise and spanwise discretisation is reduced.

Cyclic boundary conditions are set at the vertical boundaries, while velocity no-slip condition and pressure zero-gradient are imposed at the horizontal walls. All the cases are initialised with the instantaneous fields provided by a preliminary LES with the constant Smagorinsky SGS model, that has reached the statistical steady state.

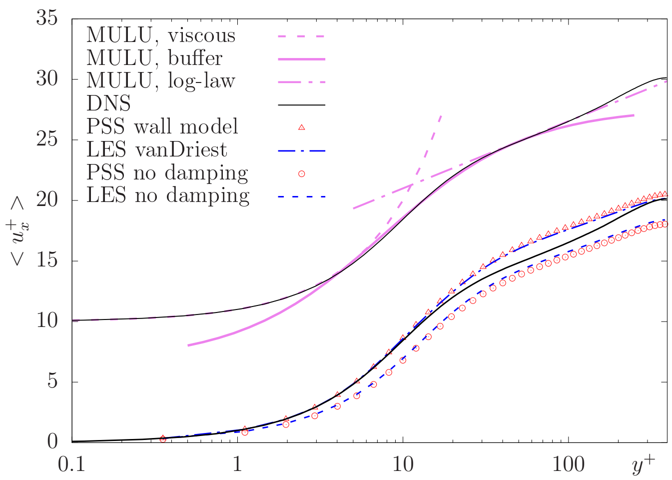

Figure 1: Non-dimensional mean velocity profiles along wall-normal direction for turbulent channel at $Re_\tau = 395$. Solid black, DNS by Moser et al. (1999). Top profiles: dash violet, analytical profile (17) derived from LU by Pinier et al. (2019). Bottom profiles: red symbols, PSS with near-wall model; red lines, LES with van Driest damping; blue symbols, PSS without near-wall model; blue lines, LES without van Driest damping.

4.3. Non-dimensional parameters

Quantities are made non-dimensional by the friction velocity u_τ and molecular viscosity ν as follow: space $x^+ = xu_\tau/\nu$, time $t^+ = tu_\tau^2/\nu$, velocity $u^+ = u/u_\tau$, variance tensor $a_{ij}^+ = a_{ij}/\nu$.

The flow is driven by a constant pressure gradient $\frac{\partial p}{\partial x} = -\rho u_\tau/\delta$; Reynolds number is set to $Re_\tau = u_\tau\delta/\nu$. The characteristic flow time is estimated to be $t_0 = U_0/2\pi\delta$, where U_0 is the bulk velocity in stream-wise direction, while the large-eddy turn over time is estimated to be $t^* = tu_\tau/\delta$.

5. Results and discussion

The following notation is adopted: if ϕ is a generic variable, then $\langle\phi\rangle$ is the time and space averaged over x, z-directions, $\phi' = \phi - \langle\phi\rangle$ is the instantaneous fluctuation and $[\phi]_{rms} = \sqrt{\langle\phi'^2\rangle}$ is the root-mean square. After the statistical steady state is reached, statistics are collected in an interval of $30t^* \sim 3t_0$ every $0.1t^*$.

5.1. Near-wall model assessment

The LU near-wall model for variance tensor is validated in the plane channel flow $Re_\tau = 395$. The computational grid is described in Table 1, and ensures a high resolution of the flow. Four simulations are performed: PSS that enforce the near-wall model, LES with van Driest damping, PSS and LES switching off the near-wall models.

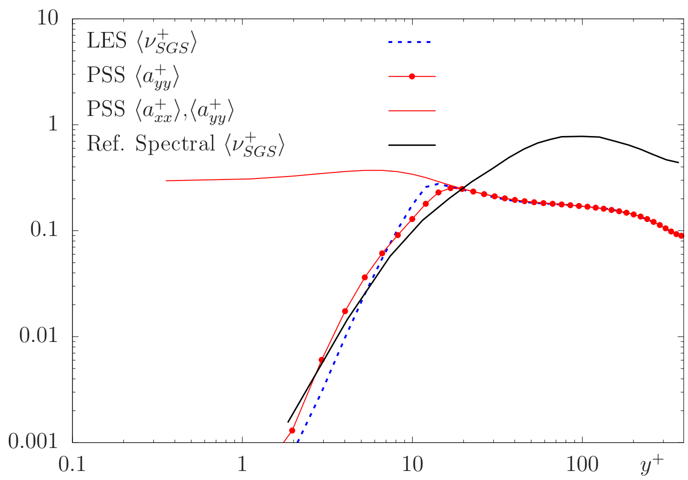

Figure 2: Non-dimensional mean eddy-viscosity parameters along wall-normal direction for turbulent channel at $Re_\tau = 395$. Dash blue, LES with van Driest damping; solid red, PSS wall-parallel components of a_{ij}; circle red, PSS wall-normal component of a_{ij}; solid black, well-resolved LES in Armenio and Piomelli (2000) with spectral code.

Figure 1 shows the non-dimensional mean streamwise velocity along vertical direction. In the top-plot, analytical expression (14) for mean velocity is compared with the DNS data: in all the three boundary layer regions, the velocity profile is correctly described. Particularly, there is a good agreement between the hyperbolic function and the reference data in the buffer layer. In the bottom-plot, the results of the simulations with and without near-wall models are reported. The data of the PSS and LES collapse one onto the other; hence they are discussed together. As expected, when the near-wall models are disabled, the velocity profile is underestimated. This is caused by a non-physical high level of eddy-viscosity near the wall (see also discussion of Figure 2), that induces a large energy dissipation. When the near-wall models are activated, velocity is well captured in the viscous and buffer layer.

Figure 2 presents the non-dimensional mean eddy-viscosity parameters for LES and PSS, respectively $\nu^+_{\mathrm{SGS}} = \nu_{\mathrm{SGS}}/\nu$ and $a^+_{ij} = a_{ij}/\nu$. Simulations are compared with the SGS eddy-viscosity profile reported in Armenio and Piomelli (2000). Such a profile is obtained from LES of the channel at $Re_\tau = 395$ with a spectral code described in Sarghini et al. (1999). The size and the discretisation of the computational domain are comparable to the one used here. The spectral code implements the Lagrangian dynamic model of Meneveau et al. (1996), where the eddy-viscosity is computed cell-by-cell, by comparing two scales of motion and minimising the model error along a fluid particle trajectory. The near-wall model has a crucial role in the correct damping of the eddy-viscosity close to the wall, both for LES and PSS. The LU near-wall model appears to accurately reproduce the slope in the region $5 < y^+ < y^+_B$, while the van Driest model exhibits a larger deflection.

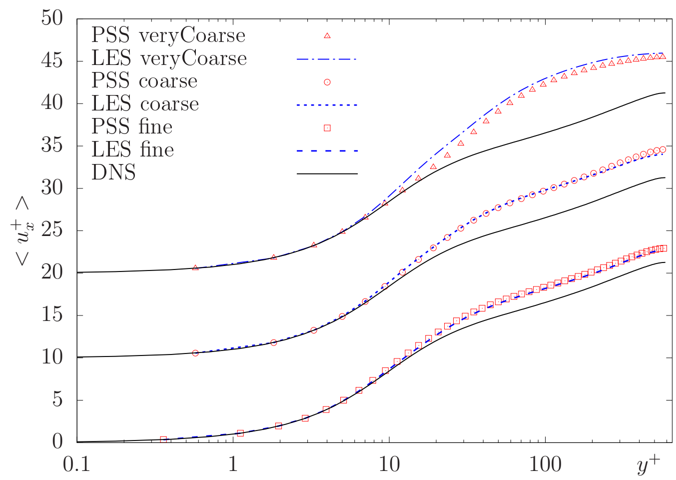

Figure 3: Non-dimensional mean velocity profiles along wall-normal direction of turbulent channel at $Re_\tau = 590$, for the three meshes described in Table 1. Solid lines, DNS by Moser et al. (1999); symbols, PSS; dash lines, LES.

Overall, the PSS with the near-wall model is able to reproduce the velocity profile as well as the LES. The eddy-viscosity profile is correctly reproduced near the wall, where the LU damping is in a good agreement with reference data. Notice that the damping is imposed only on the wall-normal component of the generalised eddy-viscosity tensor (a_{yy}), while no modification are required for the wall-parallel components a_{xx}, a_{zz}. Moreover, the only parameter to be set is the damping point y_B^+. On the contrary, the class of van Driest functions (25) are applied to all the velocity components and required to choose several empirical parameters, which leads to larger empirical content.

5.2. *Channel flow analysis*

The PSS with near-wall damping is compared with LES van Driest damping on three different meshes with a decreasing resolution in wall-parallel directions (see Table 1) at $Re_\tau = 590$.

Figure 3 displays the non-dimensional streamwise velocity component. PSS and LES practically collapse on the same values. They exhibit accurate results in the inner-region ($y^+ < 50$) for all the meshes; whereas they tend to overestimate velocity in the outer-region ($50 < y^+$). Such overestimation increases as the computational grid degrades. For a very coarse grid, the PSS shows a slightly better profile with respect to LES in the buffer layer ($10 < y^+ < 30$), as a consequent of a different damping (see Figure 5)

Figure 4 reports the root-mean square (RMS) of velocity components. In general, no significant differences are detectable between PSS and LES. As expected, the profiles are more accurate as the mesh resolution increases. The streamwise RMS is overestimated and the peak moves from the buffer layer towards the log-law region as the mesh becomes coarser and coarser. Notice that

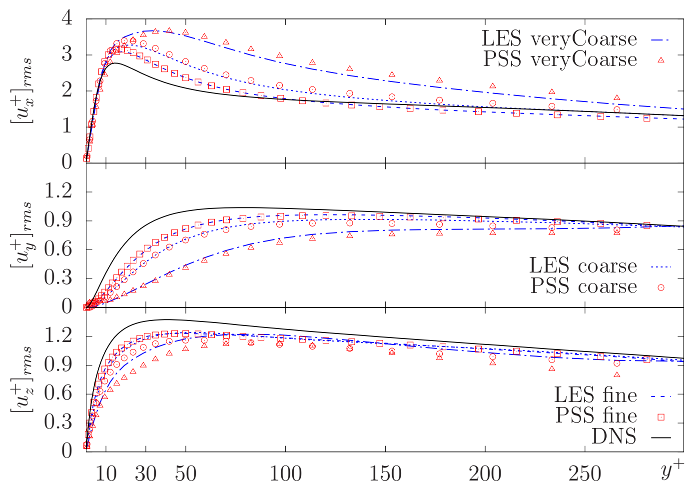

Figure 4: Non-dimensional root-mean square of velocity components along wall-normal direction of turbulent channel at $Re_\tau = 590$. Simulations with the three meshes described in Table 1. Same labels as in Figure 3.

in very coarse case, they assume lower values in the range $(10 < y^+ < 30)$ for PSS than LES. The wall-parallel RMS are globally underestimated.

Figure 5 shows the non-dimensional mean eddy-viscosity for LES and variance tensor components for PSS. The SGS eddy-viscosity and the wall-normal component a_{yy} have similar profiles, and they are discussed together below. They display common features for all the meshes used: in the viscous sublayer $(y^+ < 5)$, they are practically null; in the buffer layer $(5 < y^+ < 30)$, they rapidly increase and reach a peak in the range $y^+ \in [10, 15]$, after which a smooth decay starts. In the log-law region $(30 < y^+ < 150)$, the profiles for fine and coarse meshes decrease moderately and they eventually reduce to low values at the channel centre; the profile for very coarse mesh reports a more regular slope. For the coarse meshes, ν_{SGS} shows slightly higher values than a_{yy} near the channel center. This is possibly caused by the particular numerical implementation of the LES Samgorinsky model. However, this does not affect velocity statistics. Their values are moderate for the fine and the coarse grids (maximum 50% of the molecular viscosity), whereas they are of the same order of molecular viscosity for very coarse mesh. Hence, the SUS/SGS model plays a crucial role in this last case. The coordinates of the peaks correspond to the points where the damping starts. This is set to a fixed value $y_B^+ = 12.7$ for the LU near-wall model, while it is variable for the van Driest model. With respect to the former, the latter is activated slightly closer to the wall in the fine mesh case, about at the same point in the coarse case, and slightly further from the wall in the very coarse case. In this last case, PSS provides a higher level of eddy-viscosity which reflects on the mean velocity and the streamwise RMS profiles (see Figures 3 and 4), which are closer to the reference data in the buffer region. These results validate the pertinence of the LU wall-law model.

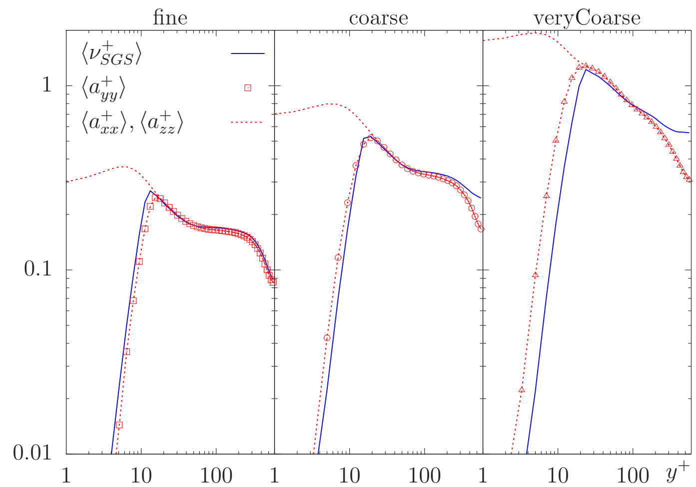

Figure 5: Non-dimensional mean eddy-viscosity parameters along wall-normal direction of turbulent channel at $Re_\tau = 590$. Simulations with the three meshes described in Table 1. Solid line, sub-grid scale eddy viscosity from LES with van Driest damping; symbols, wall-normal variance tensor component from PSS with near-wall damping; dash lines, wall-parallel variance tensor components from PSS with near-wall damping.

Figure 6 reports selected terms of the resolved TKE budget (12), averaged in time and wall-parallel planes, for the three meshes used. The time variation of TKE is made non-dimensional by the molecular viscosity. The equation for LES is obtained from (12) setting $a_{ij} = 0$, except in the dissipation term where $a_{ij} = \nu_{\text{SGS}} \delta_{ij}$ in order to account for the dissipative effect of the sub-grid model. The dissipation profiles of the PSS and LES are identical except in the region $y^+ < 20$ close to the wall, where the PSSs have lower values. This is mainly due to the fact that the wall-parallel component of variance tensor are not damped, but contribute to the energy dissipation term in equation (12). Dissipation is higher when the mesh degrades. The production terms are similar for PSS and LES: in the fine mesh case, they peak at $y^+ \simeq 15$ and $y^+ \simeq 13$ (respectively), in the coarse case they both peak at $y^+ \simeq 19$, while in the very coarse one at $y^+ \simeq 35$. It is worth to note that the PSS for the very coarse case yields a lower production close to the wall ($5 < y^+ < 20$), probably as an effect of the lower streamwise RMS (see also discussion Figure 5). The loss of energy due to SUS is only present in the pseudo-stochastic model; it assumes non-negligible negative values close to the wall ($10 < y^+$), and increases in magnitude as the mesh become coarser. It contributes to the total TKE dissipation. The turbulent compression/expansion term due to SUS is practically zero and does not contribute to the TKE budget.

5.3. Turbulent advection and compressibility

The additional terms that characterise the pseudo-stochastic model are here scrutinised. Turbulent advection (20) and the turbulent compressibility (21) are

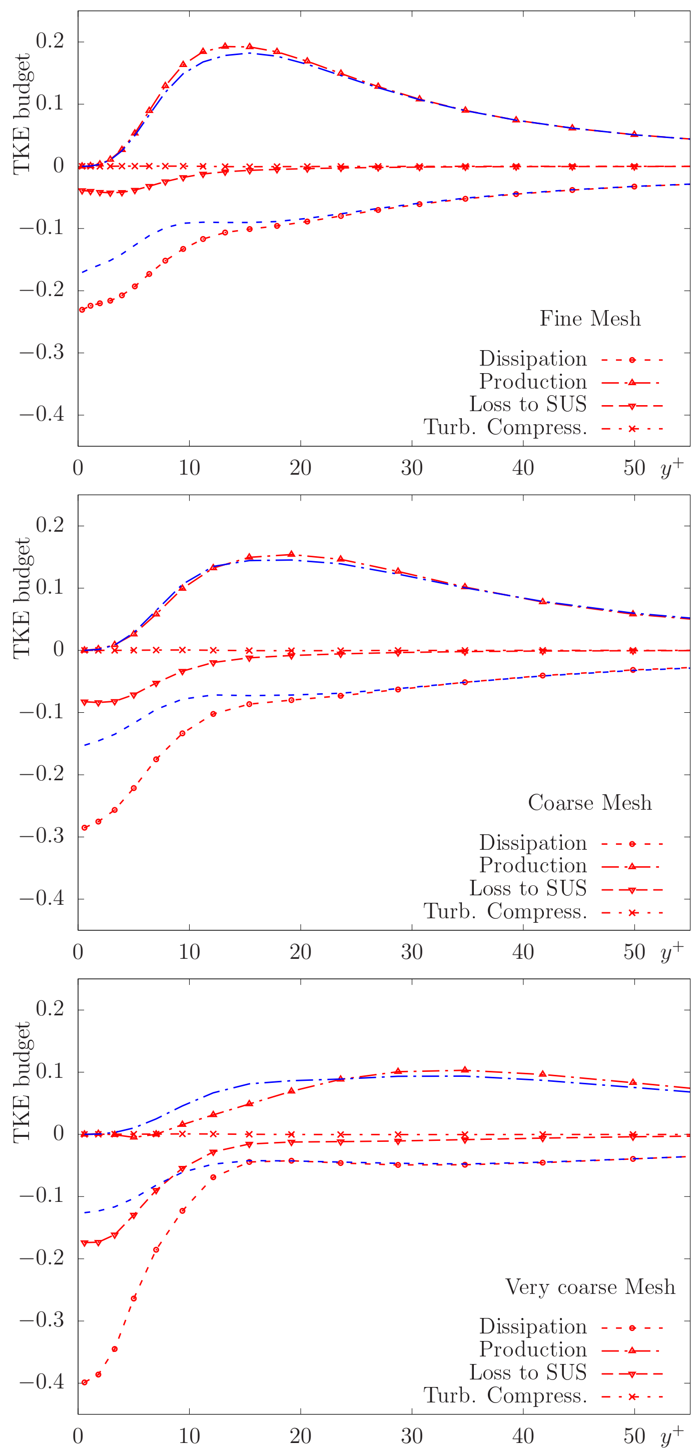

Figure 6: Non-dimensional Turbulent Kinetic Energy (TKE) budget (12) along the wall-normal direction. Simulations with the three meshes described in Table 1: from top to bottom: fine, coarse and very coarse mesh. Red lines with symbols, PSS. Blue lines without symbols, LES.

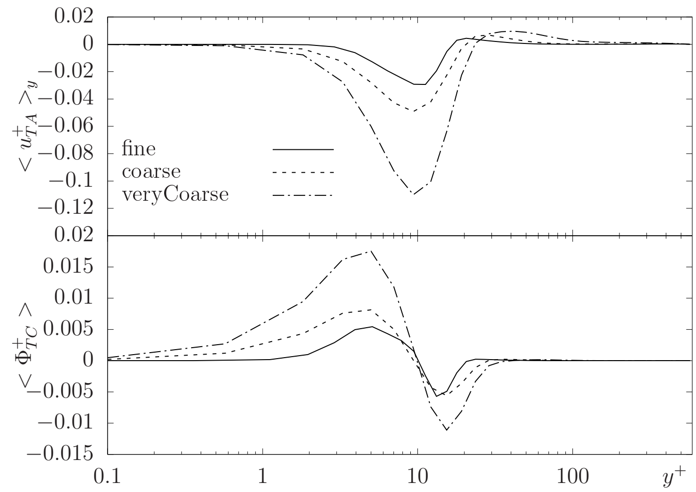

Figure 7: Non-dimensional turbulent advection (wall-normal component) u^+_{TA} and non-dimensional turbulent compressibility Φ^+_{TC} along wall distance. Average in time and wall-parallel directions. Simulations with the three meshes described in Table 1.

strongly connected with the variance tensor behaviour in Figure 5.

Figure 7 displays the wall-normal component of non-dimensional turbulent advection $u^+_{\mathrm{TA},y} = u_{\mathrm{TA},y}/u_\tau$ and the non-dimensional turbulent compressibility $\Phi^+_{\mathrm{TC}} = \Phi_{\mathrm{TC}}\nu/u_\tau^2$ along wall distance. The other components of u_{TA} are almost zero; thus, they are not reported. Globally, the magnitude of both quantities increases when the discretisation points decrease, since a larger part of the flow turbulence has to be modelled. In all the cases, wall-normal turbulent advection peaks at $y^+ = 10$ and is almost zero in the viscous sublayer and log-law region. The magnitude is quite small compared with the mean streamwise velocity: in the very coarse case, the peak of the vertical turbulent advection is 1.4% of the mean streamwise velocity at the same point. However, it generates a non-negligible vertical velocity that drives the flow towards the wall. This qualifies u_{TA} as a turbophoresis velocity, that advects the flow from a region of high to low turbulence level (quantified by the RMS velocity intensity). Turbulent compressibility presents a maximum at the end of the viscous sublayer $y^+ = 5$, and a minimum at y^+_B. It assumes moderate values. When positive (negative), it can be associated with a sort of fluid expansion (contraction) of the fluid due to turbulence.

Figure 8 shows the Φ^+_{TC} isosurfaces of negative (blue) and positive (orange) near the bottom wall, at the last time configuration. They are organised in spots elongated in the streamwise direction, confined in the buffer and viscous layer. In accordance with the mean profile, positive spots are closer to the wall, while the negative ones are immediately above. The shape and the position of these structures suggest a possible correlation with the streaks turbulent structures (e.g. see Chernyshenko and Baig (2005)); however, an additional

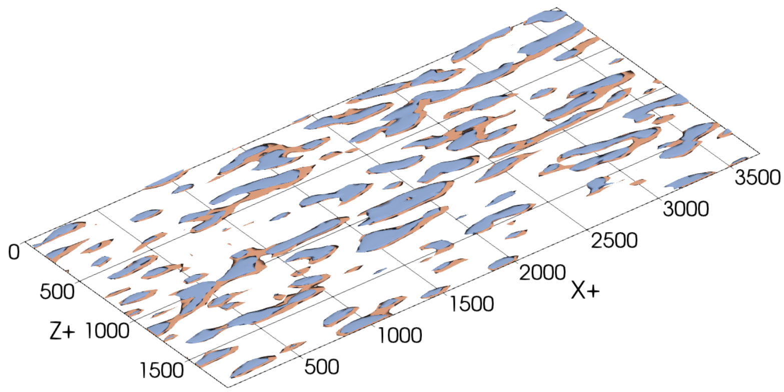

Figure 8: Positive and negative isosurfaces of Φ^+_{TC} near the bottom wall.Orange: isosurfaces $\Phi^+_{\mathrm{TC}} = 0.5\max(\Phi^+_{\mathrm{TC}}) = 0.013$. Blue: isosurfaces $\Phi^+_{\mathrm{TC}} = 0.5\min(\Phi^+_{\mathrm{TC}}) = 0.0095$.

study is required to better investigate such a correlation.

6. Conclusion

The pseudo-stochastic model introduced by Mémin (2014) is investigated both mathematically and numerically. Such a model is shown to be a generalization of the classical eddy-viscosity turbulent models, where the variance a_{ij} plays the role of an eddy-viscosity tensor. Turbulence effects are not limited to energy dissipation, but induce additional phenomena as turbulent advection and compressibility that are not usually considered. Moreover, it does not rely on the restrictive physical assumptions related to Boussinesq's hypotheses. The turbulent kinetic energy budget is derived and presented, along with a near-wall model for a_{ij} that is inferred from the analysis of boundary layer by Pinier et al. (2019). A simple isotropic constant model for a_{ij} is adopted for numerical simulation of turbulent channel flows, which are directly compared with an equivalent large-eddy simulation with the Smagorinsky model. In both cases, a near-wall damping function is used to correct the turbulent model in the proximity of the solid boundaries: the latter uses the classical van Driest function, the former employs the LU near-wall model here developed.

First, the LU near-wall model is successfully validated in the channel flow at $Re_\tau = 395$. The eddy-viscosity tensor is correctly damped and exhibits a better agreement than the van Driest function with a reference solution obtained by a highly accurate simulations model. It is worth noticing that the LU model acts only on the wall-normal direction and depends on one single parameter (theoretically estimated); in contrast to the classical model that damps eddy-viscosity for all the velocity components and requires to set several parameters. Hence, the former appears to impose a minimal correction and to have reduced empirical content. Second, the channel flow at $Re_\tau = 590$ is simulated using fine, coarse and very coarse meshes. Overall, the pseudo-stochastic simulations with the LU near-wall model are as accurate as the classical techniques. They show slightly better results when the computational grid is very coarse, since the van Driest model tends to excessively damp the eddy-viscosity. The PSS model is more effective in dissipating turbulent kinetic energy near the wall. A weak turbulent advection velocity is detectable between the viscous and buffer layer; such a velocity slightly advects the flow near the wall, form regions at high to low turbulent level (with respect to velocity RMS intensity). Hence, it is qualified as a turbophoresis phenomenon. In the same region, turbulent compressibility displays moderate positive and negative values; the visualisation of instantaneous isosurfaces suggests a possible link with the streaks turbulent structures.

Finally, the pseudo-stochastic model is a promising alternative approach for turbulent modelling, that generalises the classical models and describes a richer physics. Mathematical and numerical investigations demonstrate the potential of the model.

References

Armenio, V., Piomelli, U., 2000. A lagrangian mixed subgrid-scale model in generalized coordinates. Flow, Turbulence and Combustion 65, 51–81. doi:10.1023/A:1009998919233.

Brzeźniak, Z., Capiński, M., Flandoli, F., 1991. Stochastic partial differential equations and turbulence. Mathematical Models and Methods in Applied Sciences 1, 41–59.

Cabot, W., Moin, P., 2000. Approximate wall boundary conditions in the large-eddy simulation of high reynolds number flow. Flow, Turbulence and Combustion 63, 269–291. doi:10.1023/A:1009958917113.

Chandramouli, P., Heitz, D., Laizet, S., Mémin, E., 2018. Coarse large-eddy simulations in a transitional wake flow with flow models under location uncertainty. Computers and Fluids 168, 170 – 189. doi:doi.org/10.1016/j.compfluid.2018.04.001.

Chapron, B., Drian, P., Mémin, E., Resseguier, V., 2017. Largescale flows under location uncertainty: a consistent stochastic framework. Quarterly Journal of the Royal Meteorological Society 144, 251–260. doi:10.1002/qj.3198.

Chasnov, J.R., 1991. Simulation of the kolmogorov inertial subrange using an improved subgrid model. Physics of Fluids A: Fluid Dynamics 3, 188–200. doi:10.1063/1.857878.

Chernyshenko, S.I., Baig, M.F., 2005. The mechanism of streak formation in near-wall turbulence. Journal of Fluid Mechanics 544, 99–131. doi:10.1017/S0022112005006506.

Deardorff, J.W., 1970. A numerical study of three-dimensional turbulent channel flow at large reynolds numbers. Journal of Fluid Mechanics 41, 453480. doi:10.1017/S0022112070000691.

van Driest, E., 1956. On turbulent flow near a wall. Journal of the Aeronautical Science 23, 1007–1011. doi:10.2514/8.3713.

Durbin, P.A., Speziale, C.G., 1994. Realizability of second-moment closure via stochastic analysis. Journal of Fluid Mechanics 280, 395–407. doi:10.1017/S0022112094002983.

Flandoli, F., 2011. The interaction between noise and transport mechanisms in pdes. Milan Journal of Mathematics 79, 543–560. doi:10.1007/s00032-011-0164-5.

Frederiksen, J.S.., O'Kane, T.J., Zidikheri, M.J., 2013. Subgrid modelling for geophysical flows. Philosophical Transaction of Royal Society A 371.

Harouna, S.K., Mémin, E., 2017. Stochastic representation of the reynolds transport theorem: Revisiting large-scale modeling. Computers and Fluids 156, 456 – 469.

Holm, D.D., 2015. Variational principles for stochastic fluid dynamics. Proceedings of the Royal Society of London A: Mathematical, Physical and Engineering Sciences 471. doi:10.1098/rspa.2014.0963.

Issa, R.I., Gosman, A.D., Watkins, A.P., 1986. The computation of compressible and incompressible recirculating flows by a non-iterative implicit scheme. J. Computational Physics 62, 66.

Jasak, H., Weller, H., Gosman, A., 1999. High resolution NVD differencing scheme for arbitrarily unstructured meshes. Int. J. Numer. Meth. Fluids 31, 431–449.

Kraichnan, R.H., 1961. Dynamics of nonlinear stochastic systems. Journal of Mathematical Physics 2, 124–148. doi:10.1063/1.1724206.

Kundu, P., Cohen, I.M., 2004. Fluid Mechanics. Third ed., Elsevier Academic Press.

Kunita, H., 1997. Stochastic Flows and Stochastic Differential Equations. Cambridge University Press.

Leith, C.E., 1990. Stochastic backscatter in a subgridscale model: Plane shear mixing layer. Physics of Fluids A: Fluid Dynamics 2, 297–299. doi:10.1063/1.857779.

Leslie, D.C., 1973. Developments in the theory of turbulence. Oxford, Clarendon Press.

Lilly, D.K., 1967. The representation of small-scale tubulence in numerical simulation experiments. In: H. H. Goldstine, Proceedings of IBM Scientific Computing Symposium on Environmental Sciences , 195–210.

Mémin, E., 2014. Fluid flow dynamics under location uncertainty. Geophysical and Astrophysical Fluid Dynamics 108, 119–146. doi:10.1080/03091929.2013.836190.

Meneveau, C., Lund, T., Cabot, W., 1996. A lagrangian dynamic subgrid-scale model of turbulence. J. Fluid Mechanics 316, 353.

Métais, O., Lesieur, M., 1992. Spectral large-eddy simulation of isotropic and stably stratified turbulence. Journal of Fluid Mechanics 239, 157–194. doi:10.1017/S0022112092004361.

Mikulevicius, R., Rozovskii, B.L., 2004. Stochastic navier-stokes equations for turbulent flows. SIAM J. Mathematical Analysis 35, 1250–1310. doi:doi.org/10.1137/S0036141002409167.

Moser, R.D., Kim, J., Mansour, N.N., 1999. Direct numerical simulation of turbulent channel flow up to re_τ=590. Physics of Fluids 11, 943–945. doi:10.1063/1.869966.

Neves, W., Olivera, C., 2015. Wellposedness for stochastic continuity equations with ladyzhenskaya–prodi–serrin condition. Nonlinear Differential Equations and Applications NoDEA 22, 1247–1258. doi:10.1007/s00030-015-0321-6.

Nicoud, F., Ducros, F., 1999. Subgrid-scale stress modelling based on the square of the velocity gradient tensor. Flow, Turbulence and Combustion 62, 183–200. doi:10.1023/A:1009995426001.

Øksendal, B., 2003. Stochastic Differential Equations. Springer-Verlag Berlin Heidelberg. doi:10.1007/978-3-642-14394-6.

Oliveira, P.J., Issa, P.I., 2001. An improved piso algorithm for the computation of bouyancy driven flows. Numerical Heat Transfers, Part B. Fundamentals 640, 473.

Orszag, S.A., 1970. Analytical theories of turbulence. Journal of Fluid Mechanics 41, 363–386. doi:10.1017/S0022112070000642.

Pinier, B., Mémin, E., Laizet, S., Lewandowski, R., 2019. A model under location uncertainty for the mean velocity in wall bounded flows. Submitted to APS .

Piomelli, U., 2001. Large-eddy and direct simulation of turbulent flows. CFD2001 - 9th Conférence Annuelle de la Société Canadienne de CFD.

Piomelli, U., Ferziger, J., Moin, P., Kim, J., 1989. New approximate boundary conditions for large eddy simulations of wallbounded flows. Physics of Fluids A: Fluid Dynamics 1, 1061–1068. doi:10.1063/1.857397.

Pope, S., 2000. Turbulent Flows. Cambridge University Press.

Pope, S.B., 1983. A lagrangian two-time probability density function equation for inhomogeneous turbulent flows. The Physics of Fluids 26, 3448–3450. doi:10.1063/1.864125.

Resseguier, V., 2017. Mixing and fluid dynamics under location uncertainty. Phd thesis. University of Rennes 1 and Inria Rennes, Bretagne Atlantique (France).

Resseguier, V., Mémin, E., Chapron, B., 2017a. Geophysical flows under location uncertainty, Part I: random transport and general models. Geophysical and Astrophysical Fluid Dynamics 111, 149–176. doi:10.1080/03091929.2017.1310210.

Resseguier, V., Mémin, E., Chapron, B., 2017b. Geophysical flows under location uncertainty, Part II: quasi-geostrophy and efficient ensemble spreading. Geophysical and Astrophysical Fluid Dynamics 111, 177–208. doi:10.1080/03091929.2017.1312101.

Resseguier, V., Mémin, E., Chapron, B., 2017c. Geophysical flows under location uncertainty, Part III: sqg and frontal dynamics under strong turbulence conditions. Geophysical and Astrophysical Fluid Dynamics 111, 209–227. doi:10.1080/03091929.2017.1312102.

Resseguier, V., Mémin, E., Heitz, D., Chapron, B., 2017d. Stochastic modelling and diffusion modes for proper orthogonal decomposition models and small-scale flow analysis. Journal of Fluid Mechanics 826, 888–917. doi:10.1017/jfm.2017.467.

Sagaut, P., 2000. Large eddy simulation for incompressible flows. An introduction. Springer.

Sarghini, F., Piomelli, U., Balaras, E., 1999. Scale-similar models for large-eddy simulations. Physics of Fluids 11, 1596–1607. doi:10.1063/1.870021.